American Mineralogist, Volume 76, pages 1249–1260, 1991

Characterization and thermodynamic properties of andradite, $Ca_3Fe_2Si_3O_{12}$

MICHEL MADON
Département des Géomatériaux, Institut de Physique du Globe de Paris, 4 place Jussieu, 75252 Paris cedex 05, France
JOSÉ I. GIL IBARGUCHI, JULIÁN VIA
Departamento de Mineralogía y Petrología, Universidad del País Vasco–EHU, Aptdo. 644, 48080 Bilbao, Spain
JACQUES GIRARDEAU
Laboratoire de Pétrophysique, IPGP–Université Paris VII, 2 place Jussieu, 75251 Paris cedex 05, France

ABSTRACT

Garnet with composition of almost pure andradite ($Ca_3Fe_2Si_3O_{12}$) occurs in fissures cutting the foliation of pyroxenites at the Herbeira ultramafic massif (Cabo Ortegal, northwest Spain). The infrared and Raman spectra of the natural andradite have been recorded at room pressure and room temperature in order to model the thermodynamic properties. The IR spectrum exhibits three modes (112, 704, and 1070 cm^{-1}) not previously described in the literature. Using these new data in the lattice vibrational model of Kieffer (1979a, 1979b, 1979c), the thermodynamic properties of andradite have been calculated. Agreement between measured and calculated specific heat and relative enthalpy is excellent (ca. 1% difference between 300 and 1100 K). The specific heat ($C_{P,298} \approx 346.5$ J/mol·K) and entropy ($S_{298} \approx 313.6$ J/mol·K) at room temperature agree with reported experimental values. The model of density of state proposed for andradite is used to calculate $C_P(T)$, $H(T)$, and $S(T)$ of $Ca_3Fe_2Si_3O_{12}$ between 0 and 1500 K. Equations expressing the temperature dependence of heat capacity and relative heat content of andradite are thus proposed that allow its thermodynamic properties $C_P(T)$, $H(T)$, and $S(T)$ to be calculated at high temperatures ($T > 298$ K).

INTRODUCTION

A green gem variety of andradite garnet, often referred to as demantoid, is generally associated with serpentinites or variably retrogressed peridotites (Peters, 1963; Webster, 1970; Amthauer et al., 1974; Schmetzer et al., 1975; Fediuková et al., 1976). During the petrological study of the ultramafic Herbeira massif at the Cabo Ortegal complex (northwestern Spain), garnet with composition of almost pure andradite ($Ca_3Fe_2Si_3O_{12}$) was found associated with pyroxenites. Because the garnet family is one for which many heat capacity measurements have been performed (Berman, 1988, 1990) but for which the published experimental and theoretical values of thermodynamic parameters (C_P and S) substantially disagree (Kieffer, 1980), we have recorded infrared and Raman spectra of andradite from this area to see if another modeling scheme could be proposed and the disagreement between experimental and calculated values be explained. The results of this study along with data on the chemical composition and unit-cell parameters of garnets analyzed are presented herein.

GEOLOGICAL SETTING

The Cabo Ortegal complex is one of a series of allochthonous complexes exposed in the northwestern part of the Iberian massif as klippen of a large scale, sheetlike structure produced during the Hercynian collision (Arenas et al., 1986). In the Cabo Ortegal area, the uppermost thrust unit consists mainly of basic granulites, eclogites, and ultramafic rocks (Fig. 1). The main metamorphic event in this unit was of high-pressure, high-temperature type (garnet-clinopyroxene granulites and eclogites, Vogel, 1967; Gil Ibarguchi et al., 1990) and has been dated as Early Ordovician (Peucat et al., 1990). The ultramafic rocks comprising mainly harzburgites and pyroxenites occur in three main massifs: Limo, Herbeira, and Uzal (Girardeau et al., 1989).

Pyrope-rich garnet is often see growing at the expense of oriented spinel in pyroxenites of the Herbeira massif and seems to be related to the episode of deformation and recrystallization under high-pressure, high-temperature conditions (Girardeau et al., 1989). Andradite garnet, instead, occurs associated with chlorite and serpentine in fissures cutting across the foliation of the pyroxenite and was probably developed at the end of a retrograde greenschist episode. The actual P-T conditions under which andradite was formed cannot be estimated from the available data. They should not be higher than those conditions necessary for the development of greenschist assemblages in the pyroxenites (<450 °C).

0003–004X/91/0708–1249$02.00

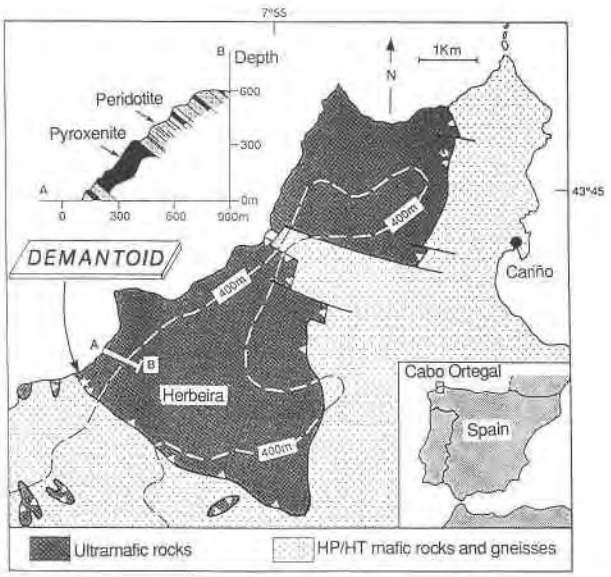

Fig. 1. Schematic geologic map of the northern part of the Cabo Ortegal complex (after Girardeau et al., 1989) with location of the Herbeira massif and andradite samples, here labeled by the varietal name demantoid. Also shown are a cross section through the pyroxenite sheet (A–B line and inset) and the 400 m contour line.

Sample description

Andradite has been found on a loose block of approximately 40 cm in diameter at the base of a cliff 500 m in height at the southeastern extremity of the Herbeira massif (Fig. 1). The block is composed essentially of slightly serpentinized, spinel-bearing clinopyroxenite. The garnet is exposed on the surface of the block, forming a crust in what must represent part of the filling of a fissure that cuts the foliation of the pyroxenite. Garnets at the surface are pale green, euhedral, millimeter-size crystals exhibiting a brilliant luster and distinct dodecahedral and trapezohedral forms and also combinations of these two forms. Toward the host pyroxenite they become finer grained, and the euhedral shape becomes less evident. The total thickness of the garnet layer is usually less than 1 cm.

Several types of garnets may be distinguished under the microscope. They correspond to different petrographic zones. From the pyroxenite toward the surface these are as follows: (1) A first zone of about 2 mm in thickness, close to the pyroxenites, with sparse garnet forming thin rims (ca. 0.05–0.1 mm) around spinel and, less often, around pyroxene crystals (Fig. 2A). Garnet around spinel tends to develop a euhedral shape and quite often exhibits a fibrous or radial aspect at the inner and middle parts and a clear, massive outer rim (Fig. 2A); it could not be ascertained whether the fibrous aspect was caused by the presence of minute radial (horse-tail) inclusions of asbestos as has been sometimes reported for this kind of garnet (e.g., Webster, 1970). Garnet also appears in this zone, rimming cavities filled by serpentine and chlorite (Fig.

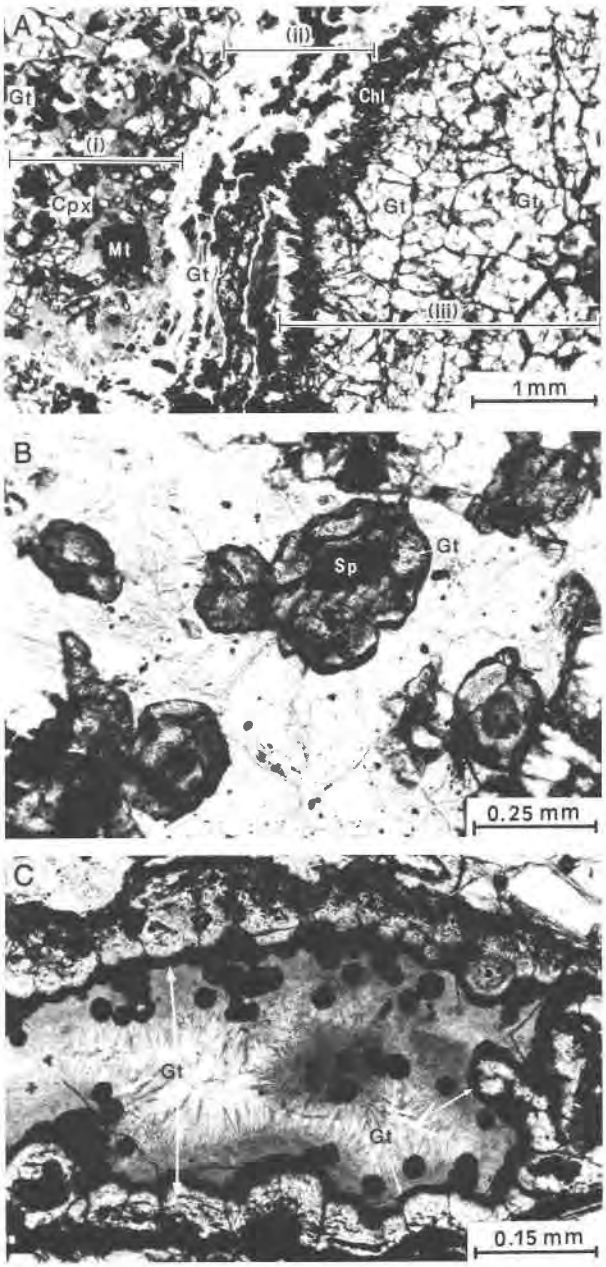

Fig. 2. (**A**) Zones 1, 2, and 3 of the garnet vein, designated as i, ii, and iii. Zone 1 is in contact with the pyroxenite host rock and contains clinopyroxene (Cpx), small garnet (Gt) around spinel, and magnetite (Mt) in a chlorite + serpentine matrix. Zone 2 contains small subhedral garnet (Gt) within chlorite + serpentine. Zone 3 exhibits a rim of radial chlorite (Chl) and progressively larger and more euhedral garnet (Gt) with increasing distance from the pyroxenite. (**B**) Small garnet (Gt) of zone 1 with an inner part rich in inclusions and a core of spinel (Sp). (**C**) Garnet (Gt) of zone 1 around spinel cores and rimming a cavity filled by serpentine and chlorite; small dark spheres within the cavity are garnet with radial aspect.

TABLE 1. Representative chemical analyses of andradite, spinel, and clinopyroxene

Sample	1r Gt.3	1c Gt.3	2r Gt.3	2c Gt.3	3c Gt.1	3r Gt.1	4 Gt.cav	Sp	Cpx
SiO_2	35.42	35.98	34.64	35.84	35.76	35.17	35.09	bd	54.34
TiO_2	0.04	bd	bd	0.03	bd	0.04	0.01	0.31	0.07
Al_2O_3	0.41	0.4	2.39	0.46	3.9	1.49	4.58	26.72	1.04
Cr_2O_3	0.11	bd	bd	0.04	2.04	0.04	bd	30.81	0.21
Fe_2O_3	30.09	30.82	27.88	30.66	23.20	28.97	25.10	11.4	bd
FeO	bd	bd	bd	bd	bd	bd	bd	22.32	2.05
MnO	bd	bd	0.1	0.02	bd	bd	bd	0.41	0.07
NiO	bd	bd	bd	bd	0.04	0.03	0.01	0.13	bd
MgO	0.04	0.07	0.11	0.06	1.54	0.2	0.78	8.94	17.32
CaO	34.13	33.58	34.01	33.79	32.89	33.97	33.7	0.02	24.46
Na_2O	bd	0.02	bd	0.01	bd	bd	bd	bd	0.07
K_2O	0.01	0.03	bd	bd	0.03	0.02	0.01	0.07	0.01
Total	100.25	100.9	99.13	100.91	99.40	99.93	99.28	101.13	96.64
FeO_{tot}	27.08	27.73	25.09	27.59	20.88	26.07	22.59	32.58	2.05
Si	2.973	3.004	2.913	2.992	2.948	2.945	2.904	bd	1.981
Ti	0.003	bd	bd	0.002	bd	0.003	0.001	0.007	0.045
Al	0.041	0.039	0.237	0.045	0.379	0.147	0.447	0.972	0.002
Cr	0.007	bd	bd	0.003	0.133	0.003	bd	0.752	0.006
Fe^{3+}	1.901	1.937	1.765	1.926	1.440	1.826	1.563	0.265	bd
Fe^{2+}	bd	bd	bd	bd	bd	bd	bd	0.576	0.062
Mg	0.005	0.009	0.014	0.008	0.189	0.025	0.096	0.411	0.941
Ni	bd	bd	bd	bd	0.0027	0.002	0.001	0.003	bd
Mn	bd	bd	0.007	0.001	bd	bd	bd	0.011	0.002
Ca	3.070	3.005	3.065	3.022	2.905	3.048	2.988	0.001	0.955
Na	bd	0.003	bd	0.002	bd	bd	bd	bd	0.005
K	0.001	0.003	bd	bd	0.003	0.002	0.001	0.003	bd

Note: Abbreviations: 1 to 4 = garnet; Gt.3 = euhedral, >1 mm andradite (zone 3); Gt.1 = smaller, radial garnet around spinel (zone 1); c = core, r = rim; Gt.cav = small garnet in cavity walls (zone 1). Sp = spinel; Cpx = clinopyroxene; bd = below detection limits of 0.01 wt%. Fe^{3+} determined by charge balance calculations: eight cations and 12 O atoms for garnet, three cations and four O atoms for spinel, four cations and six O atoms for pyroxene.

2B). (2) An intermediate zone, ca. 1 mm thick, rich in chlorite and serpentine with some minute grains of clear, massive garnets (Fig. 2C). (3) The third zone has a variable thickness between 2 and 7 mm and usually starts with a layer of chlorite perpendicular to the vein walls; it follows several layers of clear, massive garnet, progressively larger toward the outer parts of this zone (Fig. 2C). The outermost garnet may be >2 mm in diameter; the garnet crystals are euhedral and sometimes exhibit a lighter green rim. All the garnet displays anomalous birefringence. A twinning pattern consisting of six or more wedge-shaped sectors is best seen in the well-developed millimeter-size garnet of zone 3. Only the millimeter-size garnet of zone 3 has been used in the X-ray, infrared, and Raman measurements.

MINERAL CHEMISTRY

Minerals were analyzed with a Camebax Micro automated microprobe equipped with three spectrometers at the University of Clermont-Ferrand. Operating parameters included a 10 s integration time, a ca. 10-nA beam current, and a 15-kV acceleration voltage. Standards were oxides and silicates provided by the French Geological Survey (BRGM), and the ZAF correction procedure was used. Table 1 presents a selection of minerals analyzed; the complete set of data used in this report is available from J.I.G.I. on request. The procedures used to estimate Fe^{3+} contents in the minerals analyzed are indicated in the table. Thermo-gravimetric measurements of garnet were carried out in a DSC-TGA Perkin Elmer System-7 thermobalance at the University of Bilbao. A sample of approximately 25 mg of millimeter-size garnet from zone 3 was heated in N_2 atm at a rate of 10 °C min^{-1}. The initial temperature was 40 °C and the final temperature was 900 °C.

Garnet

The garnet samples analyzed are rich in andradite end-member (Table 1, Fig. 3). The main substitution in the garnet samples with diameter >2 mm from zone 3 is Al for Fe^{3+}, some samples being almost pure andradite (Figs. 3 and 4A). These garnets are practically unzoned and their Cr content is, in most cases, below the detection limits of the microprobe, which suggests that the pale-green color must be due to their content of Fe^{3+}. The thermo-gravimetric measurements did not show presence of H_2O in the structure of these garnets. The small garnets from zone 1 that grow around spinel are distinctly zoned. Their inner parts with a fibrous or radial aspect are rich in Cr, Al, or both (generally richer in these elements than the larger euhedral garnets from zone 3) and have clear, massive rims rich in Fe^{3+} (Table 1, Fig. 3). These garnets exhibit a poor correlation between $^{[6]}Al$ and Fe^{3+} (Fig. 4B) and a good negative correlation between Fe^{3+} and $^{[6]}Al + Cr$ (Fig. 4C), which may reflect Cr = Al substitution in the original spinel. These observations suggest a continuous trend, with increase in Fe^{3+} and decrease in Cr and Al, during the development of andradite-rich garnets.

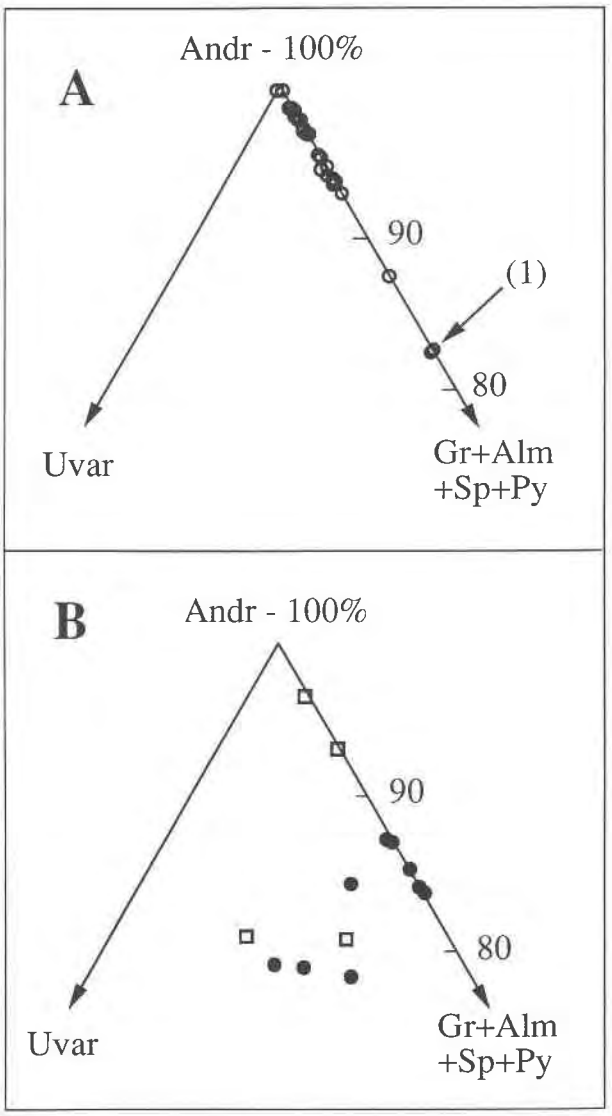

Fig. 3. Composition of garnet. (**A**) Garnet of zone 3; open circles = euhedral millimeter-size garnets; (1) = smaller garnets at the beginning of zone 3. (**B**) Garnet of zone 1; solid circles = cores, open squares = rims.

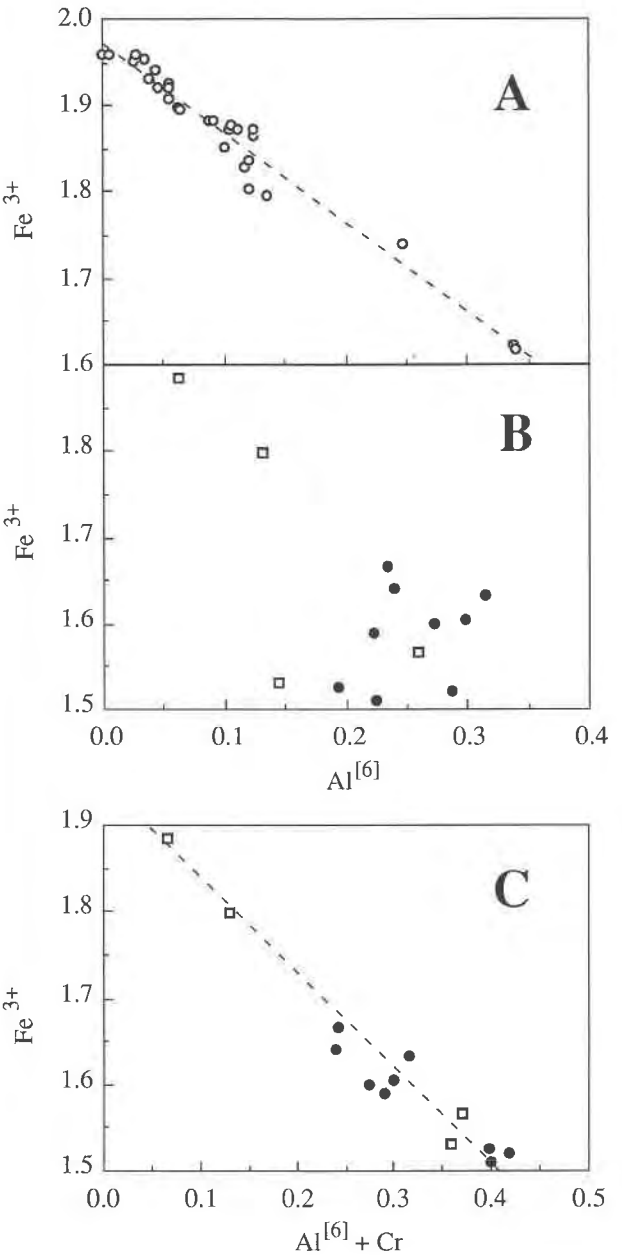

Fig. 4. (**A**) $^{[6]}Al$ vs. Fe^{3+} for garnets of zone 3; least-squares regression line is $y = 1.9717 - 1.0301x$ ($r = 0.96$). (**B**) $^{[6]}Al$ vs. Fe^{3+} for garnets of zone 1; solid circles = cores, open squares = rims. (**C**) ($^{[6]}Al + Cr$) vs. Fe^{3+} for garnets of zone 1; solid circles = cores, open squares = rims; least-squares regression line is $y = 1.9512 - 1.1055x$ ($r = 0.99$).

Pyroxene and spinel

Pyroxene has been found only in zone 1 of the andradite vein (Fig. 2C), where it may exhibit a rim of andradite (Table 1). Pyroxenes analyzed are almost pure diopside with relatively small amounts of Al, Cr, and Na. Spinel occurs generally as minute grains (<0.05 mm) in zones 1 and 2 of the andradite vein, being systematically surrounded by a rim of garnet often rich in uvarovite (Table 1, Fig. 3A). The spinel is chromite with important proportions of magnetite and spinel solutions (Table 1).

X-RAY DATA

X-ray diffraction data for andradite garnet were taken on dried material, ground to pass through a 60 μm sieve. The powder patterns were taken at room temperature with a Philips PW 1710 diffractometer (graphite monochromatized, Cu$K\alpha$ radiation). Patterns were obtained from 3 to 60° 2θ at goniometer speeds ranging from 0.2 to 2° 2θ min^{-1} with appropriate time constants, ratemeter = 5×10^2 cps at 40 kV and 20 mA. Final unit-cell parameters for the cubic mineral were obtained by least-

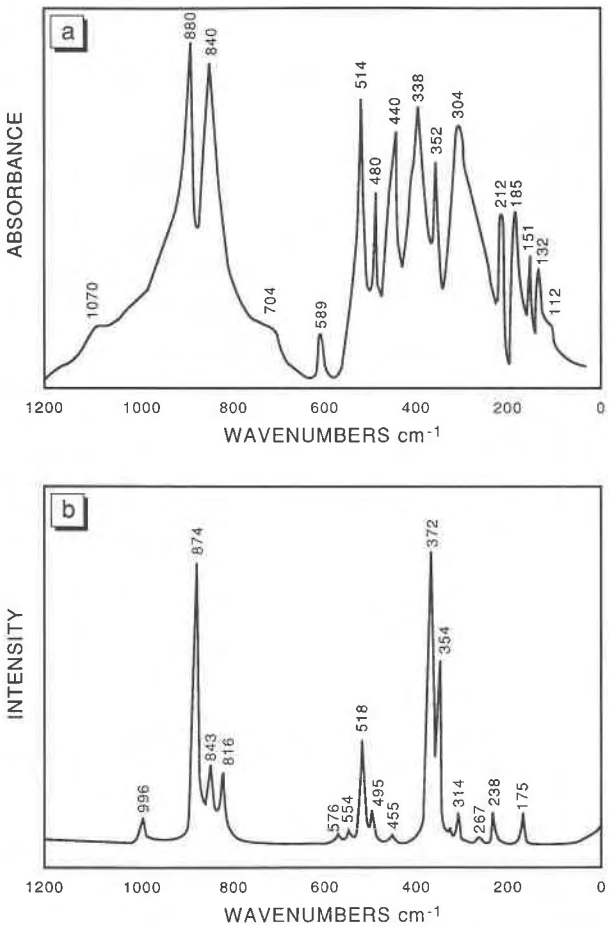

Fig. 5. Infrared (**a**) and Raman (**b**) spectra of natural andradite-rich garnet.

square refinements of the indexed powder diffraction, patterns using the LSUCRE program (Appleman and Evans, 1973). The values obtained for these parameters are a = 11.980(9) Å and V = 1719(4) Å^3. This result is slightly different from the values reported by the JCPDS (1983) for pure synthetic andradite (a = 12.059 Å, JCPDS field 10-288) and by Hazen and Finger (1989) for andradite from Val Malenco [a = 12.031(1) Å] and probably reflects the solid solution of Al for Fe^{3+}.

Thermodynamic properties of andradite from spectroscopic measurements

Spectroscopic measurements (IR and Raman) are useful for predicting, by vibrational modeling (Kieffer, 1979a, 1979b, 1979c), the thermodynamic properties of a mineral. The garnet family is one for which many heat capacity measurements have been performed (Berman, 1988, 1990) but for which the published experimental and theoretical values of thermodynamic parameters (C_P and S) substantially disagree (Kieffer, 1980). For instance, the modeling scheme of thermodynamic properties proposed by Kieffer (1980) for andradite $Ca_3Fe_2Si_3O_{12}$ leads to a value of C_P and S at 298 K of 339.4 and 292.6 J/mol·K, respectively. These values differ widely from those experimentally measured, i.e., $C^0_{P,298}$ = 351.9 and S^0_{298} = 316.4 J/mol·K (Robie et al., 1987) or $C^0_{P,298}$ = 350.6 (Kiseleva et al., 1972). To see if another modeling scheme could be proposed to explain this disagreement between experimental and calculated values, we have recorded infrared and Raman spectra of natural, nearly pure $Ca_3Fe_2Si_3O_{12}$ garnet (millimeter-size garnets of zone 3). The infrared spectrum exhibits three modes (112, 704, and 1070 cm^{-1}) not previously described in the literature. Using these new data in the lattice vibrational model of Kieffer, a value of 343.5 J/mol·K for specific heat of andradite at 298 K is obtained; if anharmonic effects are considered, a value of 346.5 J/mol·K is obtained, which is in good agreement (within about 1.5%) with the experimental values of Robie et al. (1987) and Kiseleva et al. (1972). Taking into account the magnetic contribution to the total entropy, we obtain a value of 313.6 J/mol·K for entropy at 298 K, which is very close (within less than 1%) to the experimental value of Robie et al. (1987). The model also leads to a value of the enthalpy of andradite ($H^0_{973} - H^0_{298}$ = 301.4 kJ/mol) in excellent agreement with the value recently measured (301.7 kJ/mol) by Kiseleva et al. (1989). We therefore propose a model of density of states for andradite, allowing its thermodynamic properties [$C_P(T)$, $H(T)$, and $S(T)$] to be calculated between 0 and 1500 K.

Experimental procedure

Mid- and far-infrared powder transmission spectra were obtained in CsI (mid-IR) or paraffin (far-IR) discs, using a Bruker IFS 113 FT-IR spectrometer. Spectra were recorded between 500 and 1500 cm^{-1} with a MCT detector or between 50 and 700 cm^{-1} with a liquid He–cooled bolometer detector. The amount of $Ca_3Fe_2Si_3O_{12}$ in each disc was approximately 1% (in mass). Spectra were measured at room temperature, and each spectrum results from the accumulation of 500 scans at a resolution of 2 cm^{-1}.

Raman spectra were recorded with a multichannel Raman microprobe (Dilor Microdil 28). A conventional light microscope was used to focus the laser beam (ionized Ar 1 = 5145.3 Å) into a 1-mm spot on the sample. The Raman light scattered by the sample was collected in the backscattering direction through the same objective (Leitz UTK 50). A multichannel detector (512 diodes) was used to detect and store the signal. Peak positions are located within ±1 cm^{-1}. Spectra measured at room temperature result from the accumulation of 12 spectra, the integration time being equal to 16 s.

Infrared and Raman spectra

The room-temperature and room-pressure infrared and Raman spectra of andradite are presented in Figure 5. The peak positions are listed in Table 2. The infrared spectrum recorded is in good agreement with those of andradite previously described in literature (Moore and

White, 1971; Farmer, 1974; Kieffer, 1979b), except for two reproducible weak lines appearing at 704 and 1075 cm^{-1}. The Raman spectrum agrees moderately well with that of Moore and White (1971). The six Raman modes appearing between 580 and 816 cm^{-1} in the spectrum of Moore and White are unobserved in our spectrum (Fig. 5b).

The garnet structure of andradite is cubic with 8 $Ca_3Fe_2Si_3O_{12}$ units per unit cell. The smallest Bravais cell is primitive with 4 formula units per unit cell. In this structure, the Ca atoms are eightfold coordinated, the Fe atoms sixfold coordinated, and the Si atoms fourfold coordinated. The vibrational spectra of andradite clearly possess two different groups of vibrational modes located at low and high frequency (Fig. 5). The high-frequency region extends from 816 to 996 cm^{-1} in the Raman spectrum and possesses three strong and one weak bands; it extends from 704 to 1070 cm^{-1} in the IR spectrum and possesses two strong and two weak bands. In the garnet structure, these high-frequency modes are commonly assigned to the Si-O stretching motions within $^{[4]}SiO_4$ groups (Moore and White, 1971; Omori, 1971). The low-frequency region extends from 175 to 576 cm^{-1} in the Raman spectrum (12 modes) and from 112 to 589 cm^{-1} in the IR spectrum (12 modes). The upper limit of this region (589 cm^{-1}) has been assigned as an $Fe^{3+}O_6$ octahedral mode (Omori, 1971). Indeed, the position of the top of the low-frequency region (≈620–630 cm^{-1}) does not change significantly for different garnets having Al in the octahedral site (grossularite, pyrope, spessartine, and almandine) but is substantially lower for andradite (589 cm^{-1}) that has Fe in the octahedral site. The lowest modes are not as easy to identify, but they are usually assigned as CaO_8 modes, possibly coupled with $Fe^{3+}O_6$ octahedral modes.

A critical parameter in the lattice vibrational model of Kieffer is the position of the lowest mode of the vibrational spectra. The lowest mode of andradite observed in both the IR spectrum of Moore and White (1971) and the Kieffer (1979b) IR spectrum is at 132 cm^{-1}. A weak line at 113 cm^{-1} was also observed in one sample by Moore and White (1971). In our infrared spectra (Fig. 5a), we observe the strong mode at 132 cm^{-1} but also a reproducible shoulder at about 112 cm^{-1}, which agrees with the observation of Moore and White (1971).

TABLE 2. Measured Raman and infrared absorption bands of $Ca_3Fe_2Si_3O_{12}$

Raman	Infrared
	1070*
996*	
874	880**
843	840
816**	
	704*
576	589**
554	
518	514
495	480
455	440
372	388
354	352
326	
314	304
267	
238	212
175	185
	151
	132
	112**

* Isolated Einstein oscillators.
** Cutoff of optical continuum at high and low frequency.

Vibrational modeling

Quasi-harmonic model. The lattice vibrational model of Kieffer provides a method for calculating the thermodynamic functions of a solid that is independent of any calorimetric data; the only data required are elastic wave velocities, crystallographic parameters, and spectral frequencies. To calculate the thermodynamic functions from vibrational spectra, the solid is assumed to consist of a collection of harmonic oscillators of frequency n, containing the total energy, U, of the solid. If the frequency distribution, i.e., the density of states $g(\nu)$, of the solid is known, the specific heat at constant volume, C_V, is known [$C_V = (\partial U/\partial T)_V$]. This yields (Lewis and Randall, 1961)

$$C_V(T) = 3n\mathrm{R}\int_0^{\nu} \frac{x^2 e^x}{(e^x - 1)^2}\, g(\nu)\, d\nu \qquad (1)$$

where $x = h\nu/kT$ (h being the Planck's constant, k the Boltzmann's constant, R the ideal gas constant) and n is the number of atoms in the formula unit. The $3n$R factor therefore represents the harmonic limit of the specific heat at constant volume at high temperature, i.e., the limit of Dulong and Petit.

The knowledge of C_V then leads to the specific heat at constant pressure and, consequently, to the knowledge of the enthalpy and the entropy of the solid:

$$C_P(T) = C_V(T) + T\alpha^2 V K_T \qquad (2)$$

$$H(T) - H(T_0) = \int_{T_0}^{T} C_P(T)\, dT \qquad (3)$$

$$S(T) = \int_0^T \frac{C_P(T)}{T}\, dT \qquad (4)$$

where T is the temperature, α the thermal expansion coefficient, V the molar volume of the solid, and K_T its isothermal bulk modulus.

The lattice vibrational model of Kieffer gives an estimation of the density of states, $g(\nu)$, of a solid from its spectroscopic properties. The vibrational unit of the crystal is taken as the primitive unit cell with $3n$ total degrees of freedom. Of the $3n$ degrees of freedom, three are acoustic modes and the remaining $3n - 3$ modes are optic modes. The three acoustic modes are characterized

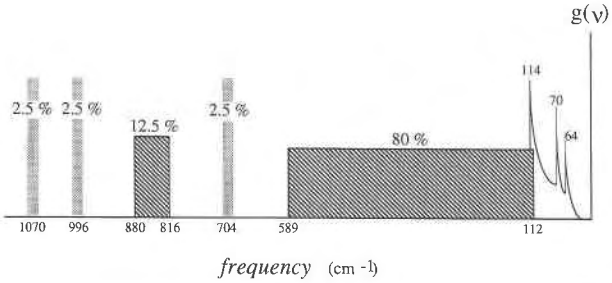

Fig. 6. Density of states $g(\nu)$ of andradite vs. frequency (cm^{-1}).

TABLE 3. Volume, thermal expansion, bulk modulus, and acoustic data for $Ca_3Fe_2Si_3O_{12}$

$V^0_{298} = 129.42$	cm^3/mol	(1)
$\alpha_0 = 2.0 \cdot 10^{-5}$	K^{-1}	(2)
$\alpha_1 = 0.8 \cdot 10^{-8}$	K^{-2}	(2)
$K_T = 159$	GPa	(3)
$V_P = 8200$	m/s	(4)
$V_S = 4820$	m/s	(4)

Note: (1) this work; (2) Skinner (1966); (3) Hazen and Finger (1989); (4) Babuska et al. (1978).

by acoustic velocities, assuming a simple sine wave dispersion of these modes toward the edge of the Brillouin zone. The $3n - 3$ optic modes span a broad range of frequencies. An estimate of the range is obtained from infrared and Raman spectra. The optic modes are distributed uniformly between a lower cutoff frequency ν_l and an upper cutoff ν_u given by spectral data. At high frequency, any isolated modes are represented as separate Einstein oscillators or by a second optic continuum. Thus, the assumed frequency distribution $g(\nu)$ is a sum of the acoustic branches, optic continuum, and Einstein oscillators (all these functions are explicitly described in Kieffer, 1979c).

Such an approach has been used to estimate the thermodynamic properties of the andradite garnet analyzed. The primitive unit cell contains four formula units, and hence there are 80 atoms and 240 degrees of freedom. The molar volume, thermal expansion, bulk modulus, and acoustic velocities used in the model are given in Table 3.

Acoustic velocities of andradite have been studied by Babuska et al. (1978). Andradite has longitudinal and shear wave velocities of 8200 and 4820 m/s, respectively. The corresponding directionally averaged acoustic velocities (Kieffer, 1979a) are $u_1 = 4627$ m/s, $u_2 = 5050$ m/s, and $u_3 = 8200$ m/s. These velocities characterize acoustic branches that reach 64, 70, and 114 cm^{-1} at the Brillouin zone boundary (Fig. 6). The acoustic modes constitute 1.25% (3/240) of the total number of degrees of freedom.

The optic modes constitute 98.75% (237/240) of the total number of degrees of freedom. From vibrational spectra (Fig. 5), these modes can be distributed among three isolated Einstein oscillators (at 704, 996, and 1070 cm^{-1}) and two optic continua, with limits given by IR and Raman spectra. The continuum at low frequency extends from 112 to 589 cm^{-1} and that at high frequency from 816 to 880 cm^{-1}. The high-frequency modes correspond to the Si-O stretching modes, which represent 20% of the total number of the optic modes (Kieffer, 1980). Eight modes (four IR and four Raman modes) are located at high frequency, and five modes (two IR and three Raman modes) are located in the frequency range 816–880 cm^{-1}. We thus assume that the continuum at high frequency contains 12.5% (⅝) of the total number of the high frequency optic modes uniformly distributed between 816 and 880 cm^{-1}, and the Einstein oscillators at 704, 996, and 1070 cm^{-1} each contain 2.5% (⅛) of the high frequency optic modes. At low frequency, the remaining optic modes (80%) are distributed uniformly in the second continuum extending from 112 to 589 cm^{-1}. The resulting model of frequency distribution, $g(\nu)$, is shown in Figure 6.

Using the density of states of Figure 6 and the parameters of Table 3, we are able to calculate the specific heat at constant volume with temperature from Equation 1 and, consequently, the thermodynamic functions $C_P(T)$, $H(T)$, and $S(T)$.

To test the accuracy of Kieffer's model, it is useful to have some calorimetric data to compare the calculated values with the experimental values. For andradite, we have used one of the two thermodynamic data sets existing on this compound, i.e., the recent heat capacity measurements obtained by Robie et al. (1987) in a large temperature range (10–1000 K). Below 365 K, heat capacity measurements were made by an intermittent heating method under quasi-adiabatic conditions using a cryostat together with a calorimeter. The accuracy of measurements was estimated to be ±0.15% above 40 K (Robie et al., 1987). The heat capacity of andradite exhibits a sharp maximum (λ peak) at about 12 K. This heat maximum arises from the antiferromagnetic ordering of the magnetic moments (spins) of the Fe^{3+} ions. Above 350 K, the heat capacity of andradite was measured by differential scanning calorimetry. Accuracy was estimated to be around ±1%. The experimental values of C_P of Robie et al. (1987) and those obtained by modeling are given in Table 4 and Figure 7. It can be seen that the model reproduces very well the calorimetric data at low temperature ($T < 200$ K), except the λ peak which cannot be observed by vibrational spectroscopy. At higher temperature ($T > 200$ K), Kieffer's model systematically underestimates heat capacities. The deviation is of about 2.5% between 200 and 1000 K (Fig. 8). The departure at high temperature of the calculated specific heat from the experimental data has been observed previously in some compounds such as Mg_2SiO_4 (Gillet et al., 1990a), SiO_2, and GeO_2 (Gillet et al., 1990b; Madon et al., 1991); it was attributed to anharmonic effects not taken into account in the quasi-harmonic model of Kieffer described previously. The calculated vibrational entropy S_v strongly differs from calorimetric data (Fig. 9). The difference results principally from the magnetic contribution to the

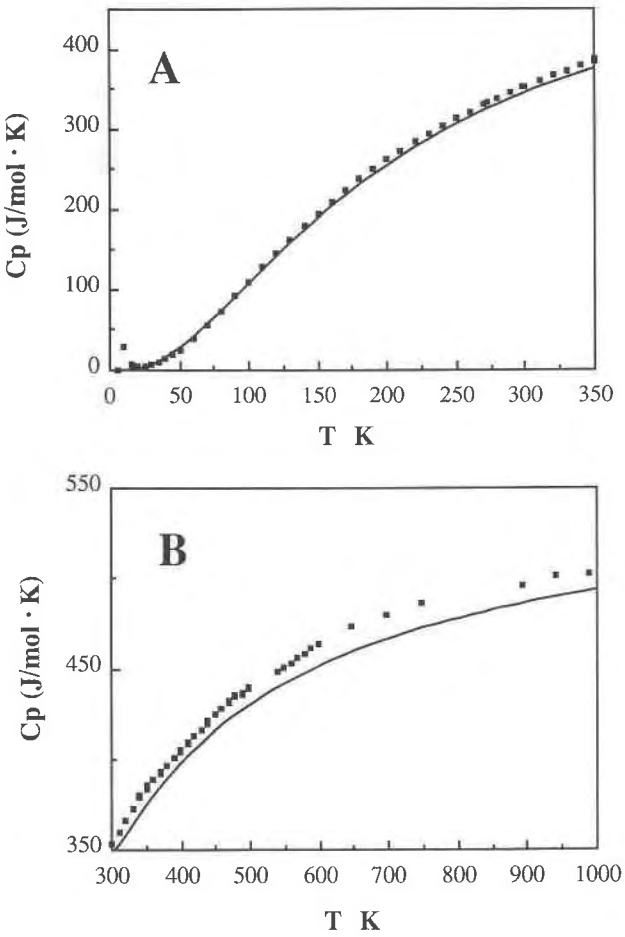

Fig. 7. Comparison of calculated (heavy line) and experimental (squares) values of heat capacity of andradite. Experimental values are from Robie et al. (1987). (**A**) Low-temperature adiabatic calorimetric data. (**B**) High-temperature ($T > 300$ K) differential scanning calorimetric data.

total entropy, which is unestimated from vibrational spectra. For andradite, the ideal magnetic entropy is ascribed to the transition from the fully antiferromagnetically ordered spin state at 0 K to the completely random spin arrangement at high temperature. There will be an increase in entropy of $2R \ln(2S + 1)$ for a first transition group ion. For Fe^{3+}, $S = 5/2$, and the ideal magnetic spin entropy for andradite is 29.8 J/mol·K. Robie et al. (1987) have shown that significant short range order must be retained by the spins at high temperature and that only 58% of the ideal magnetic entropy, i.e., 17.3 J/mol·K, contribute to the total entropy. Including this magnetic contribution S_m to the calculated vibrational entropy S_v, Kieffer's model thus reproduces the calorimetric data very well (Fig. 9). A value of 312.2 J/mol·K for entropy at 298 K is obtained, which is close (1.3%) to the experimental value (316.4 J/mol·K) of Robie et al. (1987).

The second thermodynamic data set existing on $Ca_3Fe_2Si_3O_{12}$ is that of Kiseleva et al. (1972). Measure-

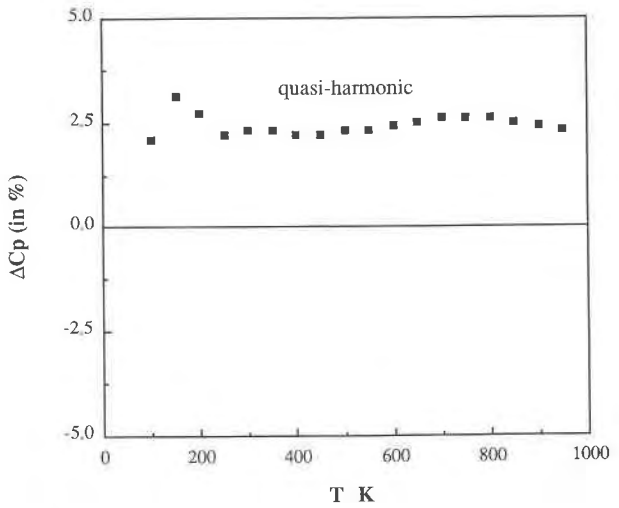

Fig. 8. Difference (in percent) between experimental values of C_P of Robie et al. (1987) and calculated values from the quasi-harmonic model of Kieffer.

ments of the change of enthalpy with temperature were made on a Tian-Calvet type microcalorimeter by heating the sample from room temperature to the temperature of the calorimeter. The accuracy of measurements was es-

TABLE 4. Values of heat capacity, vibrational entropy, and relative enthalpy of $Ca_3Fe_2Si_3O_{12}$

T (K)	C_v (J/mol·K)	C_P (J/mol·K)	S_v (J/mol·K)	$H_T - H_{298}$ (kJ/mol·K)
0	0	0	0	—
50	26.6	27.0	9.0	—
100	107.2	108.1	51.6	—
150	187.9	189.3	111.2	—
200	253.3	255.2	175.0	—
250	303.5	306.0	237.7	—
298	340.4	343.5	294.9	0
300	341.7	344.8	297.1	0.7
350	370.9	374.6	352.6	18.7
400	393.3	397.7	404.1	38.0
450	410.7	415.9	452.1	58.4
500	424.4	430.4	496.7	79.5
550	435.3	442.1	538.3	101.4
600	444.1	451.7	577.1	123.7
650	451.2	459.8	613.6	146.5
700	457.1	466.6	648.0	169.7
750	462.0	472.5	680.3	193.2
800	466.1	477.7	711.0	216.9
850	469.5	482.3	740.1	240.9
900	472.5	486.4	767.8	265.1
950	475.0	490.2	794.2	289.6
1000	477.2	493.7	819.4	314.1
1050	479.1	496.9	843.6	338.9
1100	480.8	500.0	866.8	363.8
1150	482.3	502.9	889.1	388.9
1200	483.6	505.7	910.6	414.1
1250	484.7	508.5	931.3	439.5
1300	485.8	511.2	951.2	465.0
1350	486.7	513.8	970.6	490.6
1400	487.5	516.4	989.3	516.4
1450	488.3	519.0	1007.5	542.2
1500	488.9	521.6	1025.1	568.3

Note: C_v = heat capacity at constant volume, C_P = heat capacity at constant pressure, S_v = vibrational entropy, $(H_T - H_{298})$ = relative enthalpy. Values calculated from quasi-harmonic model of Kieffer based on densities of state.

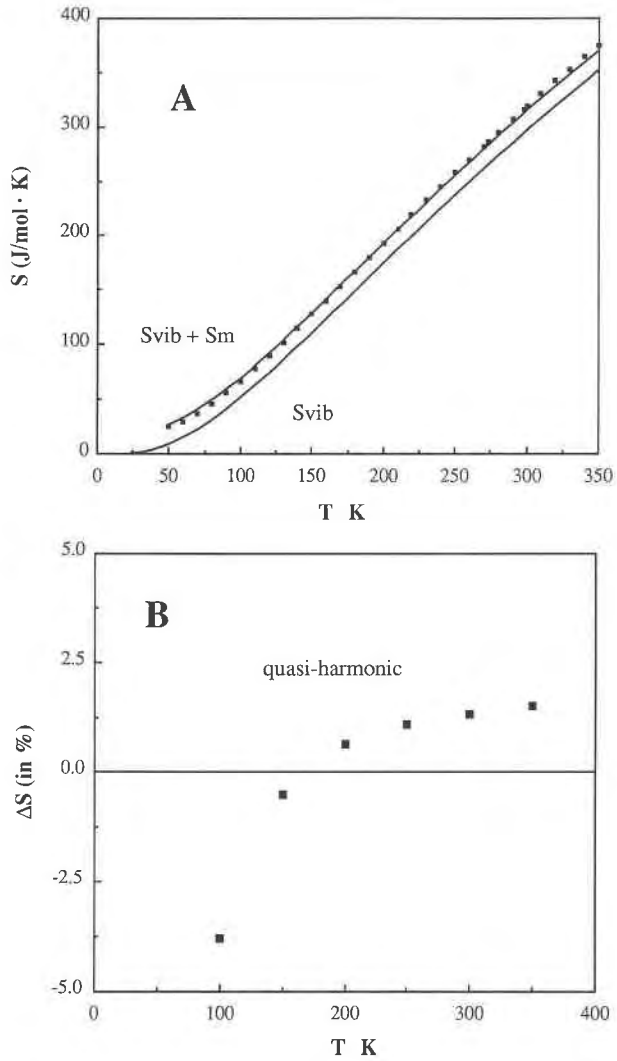

Fig. 9. (**A**) Comparison between calculated (heavy lines) and experimental (squares) values of entropy of Robie et al. (1987). Kieffer's model allows the determination of vibrational entropy (S_{vib}); the magnetic contribution (S_m) to the total entropy is about 17.3 J/mol·K. (**B**) Difference (in percent) between experimental values of S of Robie et al. (1987) and calculated values ($S_v + S_m$) from the quasi-harmonic model of Kieffer.

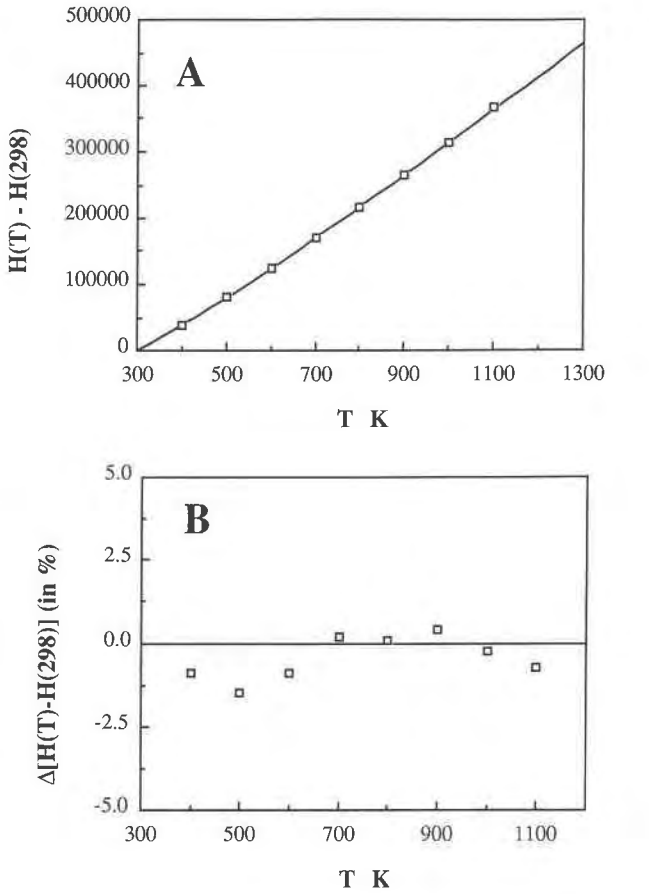

Fig. 10. (**A**) Comparison of calculated (heavy line) and experimental (squares) values of relative enthalpy of andradite. [$H(T) - H(298)$ is in J/mol]. Experimental values are from Kiseleva et al. (1972). (**B**) Difference (in percent) between experimental values of ΔH of Kiseleva et al. (1972) and values calculated from the quasi-harmonic model of Kieffer.

timated to be 1.5–2.5% (Kiseleva et al., 1972). The experimental values of ΔH of Kiseleva et al. (1972) and those obtained by modeling are shown in Figure 10. It can be seen that the model reproduces very well the calorimetric data of Kiseleva et al. (1972). The difference between experimental and calculated values is less than 1.5% between 300 and 1100 K and therefore in good agreement with the experimental error (Fig. 10B). A value of 301.4 kJ/mol for the relative enthalpy of andradite at 973 K ($H^0_{973} - H^0_{298}$) is obtained, which is in excellent agreement with the value recently measured (301.7 kJ/mol) by Kiseleva et al. (1989).

Another thermodynamic data set existing on $Ca_3Fe_2Si_3O_{12}$ is that of Devyatkova and Tikhonov (1967). They have measured the specific heat of andradite by adiabatic calorimetry between 90 and 384 K. Unfortunately, no details are given on the experimental procedure, and it is not easy to estimate the accuracy of their C_P measurements at low temperature. Moreover, their values are not very reliable because specimens were found to contain appreciable amounts of oxides that had not reacted in the synthesis (Kiseleva et al., 1989).

The proposed density of state thus satisfactorily reproduces the different calorimetric data sets for andradite but underestimates the specific heat at high temperature, which could be due to anharmonic effects not taken into account in the quasi-harmonic model of Kieffer.

Anharmonic model. Gillet et al. (1990a) have introduced a correction in the lattice vibrational model of Kieffer to consider the effects of anharmonicity. Their model accounts more readily for the observed departure at high temperature of the specific heat from the harmonic Du-

long and Petit limit ($3nR$). Anharmonicity basically results from the interactions between the normal modes of vibrations of a mineral. It can be estimated from the pressure and temperature shifts of the optical vibrational modes. A mode anharmonic parameter [$a_i = (\partial \ln \nu_i/\partial T)_V$], expressing a change with temperature (at constant volume) in the frequency of a vibrational mode ν_i, can be related to the pressure and temperature shifts of the mode by

$$a_i = \alpha \cdot (\gamma_{iT} - \gamma_{iP}) = \alpha \cdot \left(K_T \frac{\partial \ln \nu_i}{\partial P} - \frac{1}{\alpha} \frac{\partial \ln \nu_i}{\partial T} \right). \quad (5)$$

The anharmonic specific heat at constant volume C_V^* (and consequently the anharmonic specific heat at constant pressure C_P^* and the anharmonic entropy S^*) can thus be related to the harmonic specific heat (C_V) by (Gillet et al., 1990a):

$$C_V^* = \sum_{g(\nu)} \left[C_V \cdot (1 - \langle a \rangle T) - \langle a \rangle U \right] \quad (6)$$

where $\langle a \rangle$ is the mean value of the anharmonic parameters a_i of the modes ν_i, uniformly distributed in a given optic continuum (in the case of isolated modes represented by an Einstein oscillator, $\langle a \rangle$ is taken as a_i), and where U is the internal energy in excess of that at 0 K, i.e.,

$$U(T) = 3nRT \int_0^{\nu} \frac{x}{(e^x - 1)} g(\nu)\, d\nu. \quad (7)$$

This anharmonic correction in the lattice vibrational model of Kieffer leads to calculated thermodynamic properties of a solid in excellent agreement with experimental data.

Anharmonicity of garnets has been recently studied (Fiquet and Gillet, in preparation); a mean value of $-2 \cdot 10^{-5}$ K^{-1} for the anharmonic parameters a_i can be considered for the garnet family (Gillet, personal communication). This datum can thus be used to express the anharmonic thermodynamic properties $C_P^*(T)$, $H^*(T)$, and $S^*(T)$ of andradite from Equations 6, 7, 1, 2, 3, and 4. The variation of these parameters between 0 and 1500 K is listed in Table 5. The anharmonic model greatly reduces differences between calculated and experimental calorimetric data at high temperature (Figs. 11 and 12). Calculated heat capacities agree with experimental values between 300 and 1000 K within 1%, which is in good agreement with the experimental error of Robie et al. (1987) (Fig. 11B). A value of 346.5 J/mol·K for specific heat of andradite at 298 K is obtained, which is in good agreement (about 1.5%) with the experimental values of Robie et al. (1987) and Kiseleva et al. (1972) (Table 5, Fig. 11A). Taking into account the magnetic contribution to the total entropy (S_m = 17.3 J/mol·K), we obtain a value of 313.6 J/mol·K for entropy at 298 K (Fig. 12A), which is very close (less than 1%) to the experimental value of Robie et al. (1987) (Fig. 12B).

TABLE 5. Values of quasi-harmonic heat capacity, anharmonic heat capacity, and anharmonic vibrational entropy of $Ca_3Fe_2Si_3O_{12}$ calculated from anharmonic model

T (K)	C_V (J/mol·K)	C_V^* (J/mol·K)	C_P^* (J/mol·K)	ΔH^* (kJ/mol·K)	S_V^* (J/mol·K)
0	0	0	0	0	0
50	26.6	26.6	27.0	0.4	9.0
100	107.2	107.5	108.4	3.7	51.7
150	187.9	188.6	190.0	11.2	111.4
200	253.3	254.7	256.6	22.4	175.6
250	303.5	305.7	308.2	36.6	238.7
298	340.4	343.4	346.5	52.4	296.3
300	341.7	344.7	347.8	53.0	298.5
350	370.9	374.8	378.5	71.2	354.5
400	393.3	398.1	402.6	90.8	406.7
450	410.7	416.5	421.6	111.4	455.3
500	424.4	431.1	437.1	132.9	500.5
550	435.3	443.0	449.8	155.0	542.8
600	444.1	452.7	460.4	177.8	582.4
650	451.2	460.8	469.4	201.1	619.6
700	457.1	467.7	477.2	224.7	654.7
750	462.0	473.6	484.1	248.8	687.8
800	466.1	478.6	490.2	273.1	719.3
850	469.5	483.1	495.8	297.8	749.2
900	472.5	487.0	500.9	322.7	777.7
950	475.0	490.5	505.7	347.9	804.9
1000	477.2	493.7	510.1	373.3	830.9
1050	479.1	496.6	514.4	398.9	855.9
1100	480.8	499.3	518.4	424.7	879.9
1150	482.3	501.7	522.4	450.7	903.1
1200	483.6	504.0	526.2	476.9	925.4
1250	484.7	506.1	529.9	503.3	946.9
1300	485.8	508.2	533.5	529.9	967.8
1350	486.7	510.1	537.2	556.7	988.0
1400	487.5	511.9	540.8	583.6	1007.6
1450	488.3	513.6	544.4	610.8	1026.6
1500	488.9	515.3	547.9	638.1	1045.1

Note: The $\Delta H^* = H(T) - H(0)$, C_V = quasi-harmonic heat capacity at constant volume, C_V^* = anharmonic heat capacity at constant volume, C_P^* = anharmonic heat capacity at constant pressure, S_V^* = anharmonic vibrational entropy.

We thus propose, for $T > 298$ K, equations expressing the temperature dependence of specific heat (in J/mol·K) and relative enthalpy (in J/mol) of andradite that are different from those of Robie et al. (1987) and Kiseleva et al. (1972):

$$C_P(T) = 839.65 - 13.21 \times 10^{-2} T - 7.691 \times 10^{3} T^{-0.5} - 11.319 \times 10^{5} T^{-2} + 4.702 \times 10^{-5} T^{2}$$

$$H_T - H_{298} = 839.65T - 6.61 \times 10^{-2} T^{2} - 15.38 \times 10^{3} T^{0.5} + 11.319 \times 10^{5} T^{-1} + 1.567 \times 10^{-5} T^{3} + 16972.$$

CONCLUSIONS

The infrared and Raman spectra of $Ca_3Fe_2Si_3O_{12}$ have been recorded at room pressure and room temperature. The IR spectrum exhibits three modes (112, 704, and 1070 cm^{-1}) not previously used in the modeling scheme of the thermodynamic properties of andradite. Using these new data in the lattice vibrational model of Kieffer, the thermodynamic properties of andradite have been calculated. The agreement between measured and calculated

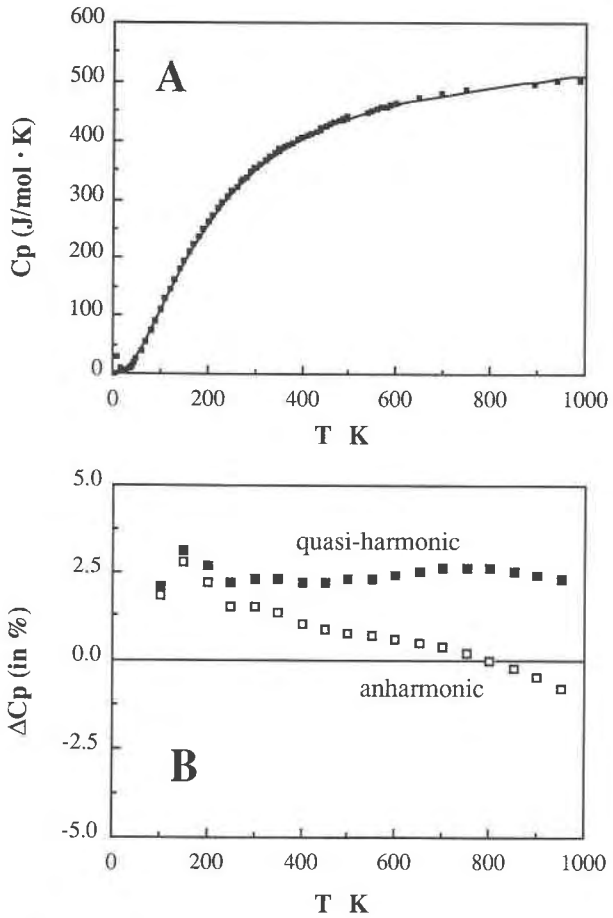

Fig. 11. (A) Comparison of experimental (squares) values of heat capacity of Robie et al. (1987) and calculated values (heavy line) from the anharmonic model. (B) Difference (in percent) among the experimental values of C_P of Robie et al. (1987) and values calculated from the quasi-harmonic model of Kieffer and the anharmonic model.

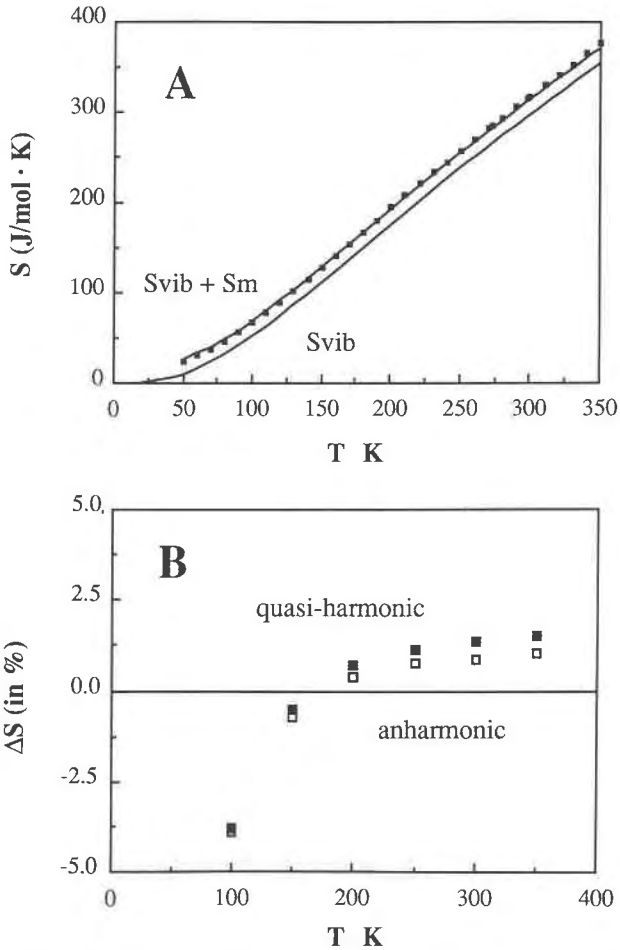

Fig. 12. (A) Comparison of experimental (squares) values of entropy of Robie et al. (1987) and calculated values (heavy lines) from anharmonic model. (B) Difference (in percent) among the experimental values of S of Robie et al. (1987) and values calculated (S_v + S_m) from the quasi-harmonic model of Kieffer and the anharmonic model.

specific heat and relative enthalpy is excellent (about 1% difference between 300 and 1100 K). The specific heat ($C_{P,298} \approx 346.5$ J/mol·K) and entropy ($S_{298} \approx 313.6$ J/mol·K) at room temperature are in good agreement with the experimental values reported by Robie et al. (1987) and Kiseleva et al. (1972). The model of density of state proposed for andradite is used to calculate $C_P(T)$, $H(T)$, and $S(T)$ of $Ca_3Fe_2Si_3O_{12}$ between 0 and 1500 K. Equations expressing the temperature dependence of heat capacity and relative heat content of andradite are thus proposed that allow its thermodynamic properties $C_P(T)$, $H(T)$, and $S(T)$ to be calculated at high temperature ($T > 298$ K).

Acknowledgments

Financial support by UPV and DGICYT grants (139.89, E040/90, 89.411) to J.I.G.I., by the French-Spanish Cooperation Project (HF-077) to J.I.G.I. and J.G., and by INSU (DBT 732AP88) to J.G. is acknowleged. The present study was done as a part of EEC contract SCI.0046. C(H). IPG contribution no. 1146, CNRS/INSU/DBT contribution no. 212.

References cited

Amthauer, G., Kurtz, W., Rost, F., and Schloemer, H. (1974) Chemismus und Genese des Andradits aus dem Serpentinit des Val Malenco (Bernina-Gebiet, Oberitalien). Schweizerische Mineralogische und Petrographische Mitteilungen, 54, 691–706.

Appleman, D.E., and Evans, H.T. (1973) Indexing and least squares refinement of powder diffraction data. NTIS Document no. PB-216188, U.S. Geological Survey, Washington, DC.

Arenas, R., Gil Ibarguchi, J.I., González Lodeiro, F., Klein, E., Martínez Catalán, J.R., Ortega Gironés, E., Pablo Maciá, J.G. de, and Peinado, M. (1986) Tectonostratigraphic units in the complexes with mafic and related rocks of the NW of the Iberian massif. Hercynica, 2, 87–110.

Babuska, V., Fiala, J., Kumazawa, M., and Ohno, I. (1978) Elastic properties of garnet solid-solution series. Physics of the Earth and Planetary Interiors, 16, 157–176.

Berman, R.G. (1988) Internally-consistent thermodynamic data for minerals in the system Na_2O-K_2O-CaO-MgO-FeO-Fe_2O_3-Al_2O_3-SiO_2-TiO_2-H_2O-CO_2. Journal of Petrology, 29, 445–522.

——— (1990) Mixing properties of Ca-Mg-Fe-Mn garnets. American Mineralogist, 75, 328–344.

Devyatkova, E.D., and Tikhonov, V.V. (1967) Teploprovodnoct' i teploemkost' ittrii-kal'tsievykh granatov (in Russian). Fizika Tvergodo Tela, 9, 772–777.

Farmer, V.C. (1974) Orthosilicates, pyrosilicates and other finite chain silicates. In V.C. Farmer, Ed., The infrared spectra of minerals, monograph 4, p. 285–303. Mineralogical Society, London.

Fediuková, E., Hovorka, D., and Gregus, J. (1976) Compositional zoning of andradite from serpentinite at Dobsiná (West Carpathians). Vestnik Ustredniho Ustavu Geologickeho, 51, 339–345.

Gil Ibarguchi, J.I., Mendia, M., Girardeau, J., and Peucat, J.J. (1990) Petrology of eclogites and clinopyroxene-garnet metabasites from the Cabo Ortegal complex (northwestern Spain). Lithos, 25, 133–162.

Gillet, Ph., Guyot, F., and Malezieux, J.M. (1990a) High pressure and high temperature Raman spectroscopy of Ca_2GeO_4: Some insights of anharmonicity. Physics of the Earth and Planetary Interiors, 58, 541–554.

Gillet, Ph., Le Cléac'h, A., and Madon, M. (1990b) High temperature Raman spectroscopy of SiO_2 and GeO_2 polymorphs: Some insights on anharmonicity and thermodynamic properties of the SiO_2 polymorphs at high temperatures. Journal of Geophysical Research, 95, 21635–21655.

Girardeau, J., Gil Ibarguchi, J.I., and Ben Jamaa, N. (1989) Evidence for a heterogeneous upper mantle in the Cabo Ortegal Complex, Spain. Science, 245, 1231–1233.

Hazen, R.M., and Finger, L.W. (1989) High-pressure crystal chemistry of andradite and pyrope: Revised procedures for high-pressure diffraction experiments. American Mineralogist, 74, 352–359.

Joint Committee for Powder Diffraction Standards (JCPDS) (1983) Group data book. International Centre for Diffraction Data, Swarthmore, Pennsylvania.

Kieffer, S.W. (1979a) Thermodynamics and lattice vibrations of minerals. 1—Mineral heat capacities and their relationships to simple lattice vibrational models. Review of Geophysics and Space Physics, 17, 1–19.

——— (1979b) Thermodynamics and lattice vibrations of minerals. 2—Vibrational characteristics of silicates. Review of Geophysics and Space Physics, 17, 20–34.

——— (1979c) Thermodynamics and lattice vibrations of minerals. 3—Lattice dynamics and an approximation for minerals with application to simple substances and framework silicates. Review of Geophysics and Space Physics, 17, 35–38.

——— (1980) Thermodynamics and lattice vibrations of minerals. 4—Application to chain and sheet silicates and orthosilicates. Review of Geophysics and Space Physics, 18, 862–886.

Kiseleva, I.A., Topor, N.D., and Mel'chakova, L.V. (1972) Experimental determination of heat content and heat capacity of grossularite, andradite and pyrope. Geokhimiya, 11, 1372–1379 (in Russian).

Kiseleva, I.A., Ogorodova, L.P., and Sokolova, Y.L. (1989) The enthalpy of formation of andradite. Geokhimiya, 1, 125–131.

Lewis, B.N., and Randall, M. (1961) Thermodynamics, 723 p. McGraw-Hill, New York.

Madon, M., Gillet, Ph., Julien, Ch., and Price, G.D. (1991) A vibrational study of phase transitions among the GeO_2 polymorphs. Physics and Chemistry of Minerals, in press.

Moore, R.K., and White, W.B. (1971) Vibrational spectra of the common silicates: I. The garnets. American Mineralogist, 56, 54–71.

Omori, K. (1971) Analysis of the infrared absorption spectrum of almandine pyrope garnet from Nisojan, Osaka prefecture, Japan. American Mineralogist, 56, 841–849.

Peters, T. (1963) Mineralogie und Petrographie des Totalpserpentins bei Davos. Schweizerische Mineralogische und Petrographische Mitteilungen, 43, 529–685.

Peucat, J.J., Bernard-Griffiths, J., Gil Ibarguchi, J.I., Dallmeyer, R.D., Menot, P., Cornichet, J., and Iglesias Ponce de Leon, M. (1990) Geochemical and geochronological cross-section of the deep Hercynian crust: The Cabo Ortegal high-pressure nappe (NW Spain). Tectonophysics, 177, 263–292.

Robie, R.A., Bin, Z., Hemingway, B.S., and Barton, M.D. (1987) Heat capacity and thermodynamic properties of andradite garnet, $Ca_3Fe_2Si_3O_{12}$, between 10 and 1000 K and revised values for ΔG^0_m(298.15 K) of hedenbergite and wollastonite. Geochimica et Cosmochimica Acta, 51, 2219–2224.

Schmetzer, K., Traub, I., and Medenbach, O. (1975) Demantoid aus Korea. Zeitschrift der Deutsche Gemmologischen Gesellschaft, 24, 1–3.

Skinner, B.J. (1966) Thermal expansion. Geological Society of America Memoir, 97, 75–96.

Vogel, D.E. (1967) Petrology of an eclogite and pyrigarnite bearing polymetamorphic rock complex at Cabo Ortegal, NW Spain. Leidse Geologische Mededelingen, Leiden, 40, 121–213.

Webster, R. (1970) Gems, their sources, descriptions and identification, 836 p. Butterworth, London.

Manuscript received January 2, 1990
Manuscript accepted March 15, 1991